



Transient Stability Enhancement of Multi-Machine Hybrid Power System Employing Modified Series Resonance type Fault Current Limiter

Chintan R. Mehta¹ and Santosh C. Vora²

¹Assistant Professor, Department of Electrical Engineering,
Institute of Technology, Nirma University, Ahmedabad (Gujarat), India.

²Professor & Head, Department of Electrical Engineering,
Institute of Technology, Nirma University, Ahmedabad (Gujarat), India.

(Corresponding author: Santosh C. Vora)

(Received 22 April 2020, Revised 15 June 2020, Accepted 15 June 2020)

(Published by Research Trend, Website: www.researchtrend.net)

ABSTRACT: The increased penetration of renewable energy-based generation calls for stability studies - most vital for the power system. During the fault duration, the challenge is to restrict the short circuit current and maintain the bus voltage at wind farm within the limits specified by respective grid codes. According to literature available, fault current limiter is one of the techniques to augment the transient stability of grid-connected generators. This paper discusses the implementation of a series resonance type fault current limiter to enhance the transient stability of a multi-machine power system considering hybrid sources of power generation i.e. synchronous generator, doubly fed induction generator-based wind farm and PV based solar farm. The authors have implemented the modified series resonance type fault current limiter in a modified western system coordinating council 3 generators 9 bus system to analyze the system behaviour in case of a symmetrical fault at a weak load bus. To check the effectiveness of the proposed technique, its performance is compared with the other fault current limiters proposed in the literature, and results are encouraging & discussed in this paper.

Keywords: Doubly Fed Induction Generator (DFIG), Fault current limiter, Multi-machine Power System, PV based Solar Farm, Synchronous Generator, Transient stability.

Abbreviations: CBFCL, Capacitive bridge type fault current limiter; DVR, Dynamic voltage restorer; DFIG, Doubly fed induction generator; FACT, Flexible ac transmission; FCL, Fault current limiter; GSC, Grid side converter; HPFC, Hybrid power low controller; LVRT, Low voltage ride through; PRBFCL, Parallel resonance bridge type fault current limiter; PCC, Point of common coupling; PSS, Power system stabilizer; PV, Photo-voltaic; RSC, Rotor side converter; SMIB, Single machine infinite bus; SSSC, Static series synchronous compensator; STATCOM, Static synchronous compensator; SVC, Static var compensator; UPFC, Unified power flow controller; VSWT, Variable speed wind turbine; WPP, Wind power plants.

I. INTRODUCTION

The clean and green energy resources now offer affordable electricity access to all and reduce the carbon footprint with the enabling technologies. The bulk of renewable energy-based power generation in the world today is achieved mainly by extracting solar energy and wind energy. The declining cost of photovoltaic (PV) cells is driving the exponential growth of solar energy-based generation. It is projected that solar energy production will attain the top spot and will cater to 28% of world energy demand by 2040 [1]. On the other side, wind energy has been widely accepted by many countries and is a fast-developing energy source. Its adoption is increasing due to its low maintenance cost, maximum power extraction, size and control offered by the converters, no air pollution, and availability in several parts of the world. It is reported that throughout the world, a total of 760 GW of the wind power will be generated by the end of the year 2020 [2]. The Indian government has also planned to generate almost 175GW of power from renewable energy sources including 100 GW from solar energy and 60 GW from wind energy by the year 2022 albeit many challenges associated with the integration of wind and solar

generation with the power grid [3,4]. One of the major requirements for the power system operation is to keep the system in a state of operating equilibrium and to recover to an acceptable state of equilibrium after being subjected to disturbances.

The transient stability study plays a significant role in understanding the continuity of power flow and proper control of the power system having multiple renewable sources connected to it. While the bulk power generation incorporates renewable energy sources viz. Induction generators (in wind farms) and PV cells (in solar farms), ensuring the system transient stability is of utmost importance since the characteristics of preceding sources are much different compared to synchronous generators.

Amongst the available wind generation options, doubly-fed induction generators (DFIG) are popular [5]. In DFIG the stator winding is directly connected to the grid, whereas the rotor is connected to the grid (via rotor side converter (RSC), DC link, and grid side converters (GSC)) to offer flexibility for machine control. At the instance of near-end fault, DFIG's terminal voltage drops below the nominal value, the output power reduces accordingly, but the mechanical power input remains unchanged leading to speeding of the turbine -

generator. Moreover, high fault current flows through the converters of DFIG which will affect the life of the converters [6, 7]. On the other hand, the occurrence of grid faults causes the imbalance between PV generated power and power inserted by voltage source inverter (VSI) to the grid. Due to this imbalance of the power, the intermediate DC link voltage is increased sharply and current in AC side of VSI increases damaging the power electronic interface [8]. Further, large scale penetration of renewable energy sources into the power grid modifies the system short circuit level, which may demand the reconsideration of circuit breaker rating and revision in relay settings.

To overcome these challenges and ensure the stability of the power system with large penetration of renewable energy sources, researchers are mining various solutions.

According to the latest grid code requirements, wind farms and solar farms should stay connected to the system network even during fault [9] and should supply the reactive power support to the system to improve the voltage profile at the point of common coupling (PCC). Patel *et al.*, have shown the effects of various FACTS devices like SSSC and UPFC on distributed system considering wind farm [10]. The use of static synchronous compensator (STATCOM) for improvement of transient stability of the hybrid power system is proposed by the authors of [11, 12]. The STATCOM supplies the required reactive power to improve the voltage profile of the system, but the STATCOM cannot limit the fault current. Hence the converters of DFIG and PV solar array will be at risk due to high fault current. Moreover, the cost of STATCOM is also a hindrance in using it extensively in the power system. The authors of [13] have proposed and compared three different configurations of the hybrid power flow controller (HPFC) for a multi-machine power system. HPFC topology is a mixture of a shunt connected controllable source of reactive power, and two series-connected voltage sourced converters on each side of the shunt device. A common dc link has been provided to exchange active power. The authors have not shown the effects of the proposed power flow controller on the active power output of various generators as well as on the magnitude of current at the instance of disturbance in the system. For the standalone PV system, the adaptive observer-based control strategy is proposed by authors of [14], and the sliding mode control strategy is proposed by authors of [15] for improvement in fault ride through capability of PV farm connected with the grid. The authors of [14,15] have not shown the impact of the proposed control strategy on a hybrid power system having multiple generators. The application of proportional and integral (PI) controllers in PV and wind farm controllers and a combination of power system stabilizers (PSS) and static series synchronous compensator (SSSC) controllers for improvement in transient stability of IEEE 68 bus system is proposed by Movahedi *et al.*, [16]. The authors have proposed an adaptive velocity update relaxation particle swarm optimization algorithm compared it with a genetic algorithm. The authors of [17] have compared the PSS1A and PSS4B on transient stability improvement in the diesel-wind-solar PV system. Ghanasyam *et al.*, have proposed the modification in the controllers of the converters of the

DFIG and solar PV system to allow maximum reactive power injection during the fault period in the multi-machine power system in [18]. The suggested modification improves the voltage profile but fails to reduce the fault current. The literature discussed so far uses mainly PSS, FACTS devices like STATCOM, SVC, SSSC, etc. to improve the transient stability in a multi-machine power system having multiple renewable energy-based generators. The major drawback of these systems is higher cost and these techniques mainly improve voltage profile by reactive power compensation. The other technique proposed in the literature to improve LVRT performance and transient stability of the power system is by using fault current limiters (FCL)[19,23]. The use of FCLs not only improves the transient stability of the wind farm connected to the grid but also reduces the peak current at the instance of fault thus protecting the converters of DFIG.

The authors in this paper have presented a modified series resonance type fault current limiter [MSRFCL]. This modified FCL is compared with the capacitive bridge type fault current limiter (CBFCL) and parallel resonance bridge type fault current limiters (PRBFCL) proposed in the literature. The effectiveness of the MSRFCL is discussed in the multi-machine system by considering the modified western system coordinating council (WSCC) 3 generator 9 bus system. To show the effect of higher penetration of renewable energy sources in the proposed system, the synchronous generator at bus 2 is replaced by equal capacity aggregated coherent DFIG based wind farm, while the synchronous generator at bus 3 is replaced by the equal capacity of solar PV farm. The symmetrical fault (3L-G) is simulated at the weakest load bus of the system and the effectiveness of MSRFCL is presented in the following.

The paper is organized as follows.

- (1) Section II gives an Equivalent circuit of various generators and its modelling concepts and effects of fault in the power system.
- (2) Section III discusses the concept and operation of fault current limiters.
- (3) Section IV represents the discussion on the modified WSCC 3 generator 9 bus system.
- (4) Section V discusses the selection of various parameters for FCL.
- (5) Section VI discusses the simulation results and the comparison of various FCLs.
- (6) Section VII summarizes the research work followed by the research scope in Section VIII.

II. EQUIVALENT CIRCUIT AND MODELLING OF VARIOUS SOURCES

A. Equivalent circuit and system modelling of Induction generator

Fig. 1 shows the equivalent circuit of DFIG for short circuit analysis.

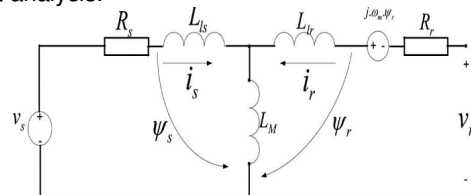


Fig. 1. Equivalent circuit of DFIG for short circuit analysis [24].

In this model, the rotor variables are referred to the stator side for simplicity.

Using motor convention, the stator voltage and rotor voltage in *abc* frame can be expressed as,

$$\vec{v}_s = R_s \vec{i}_s + \frac{d\vec{\psi}_s}{dt} \quad (1)$$

$$\vec{v}_r = R_r \vec{i}_r + \frac{d\vec{\psi}_r}{dt} - j\omega_m \vec{\psi}_r \quad (2)$$

Here stator flux and rotor flux are given by

$$\vec{\psi}_s = L_s \vec{i}_s + L_m \vec{i}_r \quad (3)$$

$$\vec{\psi}_r = L_r \vec{i}_r + L_m \vec{i}_s \quad (4)$$

In this case, $L_s = (L_{ls} + L_m)$ and $L_r = (L_{lr} + L_m)$.

In the above equations, stator and rotor resistances are represented by R_s & R_r respectively, ω_m represents slip angular frequency, stator and rotor self-inductance are represented by L_s & L_r respectively, while L_{ls} , L_{lr} and L_m are stator leakage reactance, rotor leakage inductance, magnetizing inductance respectively. \vec{v}_s & \vec{v}_r represents stator and rotor voltages respectively, $\vec{\psi}_s$ & $\vec{\psi}_r$ are the stator and rotor flux linkages and \vec{i}_s & \vec{i}_r represents stator and rotor currents respectively. To derive the rotor over-current during the short circuit, the rotor voltage is the most important variable from the converter point of view. This voltage is induced by the stator flux variation, and it can be calculated by deriving \vec{i}_s from (3) and substituting into (4):

$$\vec{v}_r = \frac{L_m}{L_s} \vec{v}_s - \sigma L_r \vec{i}_r \quad (5)$$

Here σ is the leakage factor. It is given as $\sigma = 1 - \frac{L_m^2}{L_s L_r}$.

Thus the rotor voltage can be found by combining (2) and (5)

$$\vec{v}_r = \frac{L_m}{L_s} \left(\frac{d}{dt} - j\omega_m \right) \vec{\psi}_s + \left(R_r + \sigma L_r \left(\frac{d}{dt} - j\omega_m \right) \right) \vec{i}_r \quad (6)$$

The rotor voltage given in (6) can be divided into two terms. The first term represents open-circuit voltage (\vec{v}_{r0}) which depends on the stator flux and the second term is smaller and it is caused by the voltage drop on both the rotor resistance R_r and the rotor transient inductance σL_r . From (6), when there is no current in the rotor circuit, the rotor voltage due to the stator flux is (\vec{v}_{r0}), as depicted in (7).

$$\vec{v}_{r0} = \frac{L_m}{L_s} \left(\frac{d}{dt} - j\omega_m \right) \vec{\psi}_s \quad (7)$$

The detailed analysis of voltages under steady-state and under faulty conditions is given in [24]. It can be further noted that the DC link voltage is controlled by GSC and the active and reactive power of the system are controlled by the RSC with rotor circuit current control. The RSC and GSC operate as voltage-source converters (VSC).

B. Modelling of PV system

A 3-phase, 2-stage grid-connected solar PV system is shown in Fig. 2.

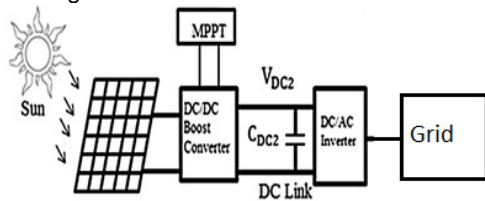


Fig. 2. Block diagram of grid-connected solar PV system [8].

It consists of DC/DC boost converter in the first stage while in the second stage it consists of DC/AC grid-connected voltage source inverter (VSI).

The total power flow through the PV system can be given by

$$P_{PV} = P_{DC2} + P_g \quad (8)$$

Where P_{DC2} represents the power flow through the DC link capacitor (C_{DC2}) of the PV system and P_g is the power injected by the inverter in the grid. P_{PV} is the total power output of PV arrays. For the normal operation, the DC power generated by the PV farm (P_{PV}) is equal to the AC power delivered to the grid (P_g), provided power electronic converter losses are neglected.

Hence,

$$P_{PV} = P_g = 3 V_g I_g \quad (9)$$

Here V_g and I_g represent the RMS value of phase voltage and phase current respectively. The PV DC link voltage is constant considering the power balance under steady-state condition.

At the instance of a near-end fault, the DC link voltage increases abruptly, as DC power output from the PV arrays cannot be injected to the grid, due to severe voltage dip at PCC. To overcome the sharp rise in DC link voltage, researchers have proposed PI controller based non-MPPT strategy. According to this strategy, the MPPT controllers are bypassed at the instance of the fault and the active power insertion in the grid is reduced. This strategy also inserts reactive current through the inverters in the system to improve the voltage profile of the system without exceeding the maximum current limit of inverters. The control scheme of the PV solar array is deliberated [8].

C. Modelling of Synchronous Generator

The synchronous generator modeling with controllers is very well known and not reproduced here. Its voltage, current and flux linkage expressions during normal, as well as fault conditions, are deliberated in many literatures [25, 26].

D. Effect of fault in power system

At the instance of fault in the power system network, the fault current is supplied from power sources to the faulty node due to a huge voltage sag at the faulty node. This phenomenon causes very small active power and voltage generation at the rotating machines (DFIG & SG). It will create instability in the system as the power balance equation will not be followed. This situation can be explained by the swing equation [8] as follows.

$$\frac{2H}{\omega} \frac{d^2 \delta}{dt^2} = P_m - P_e \quad (10)$$

Here P_m represents the mechanical power input, P_e represents the electrical power output, δ denotes the rotor angle and H is the inertia constant of the machine. The overall inertia of the system is reduced due to solar PV farm as the solar farm has zero inertia and Induction machines demand inertia emulation. The FCL introduces additional resistance during the fault causes the stator voltage of DFIG and SG to be developed due to voltage drop across the resistance of the FCL. The delivery of the electrical power is maintained by generators of the system and the desired power balance is achieved.

III. CONCEPT AND OPERATION OF FAULT CURRENT LIMITERS (FCLs)

To improve the transient stability of the power system having hybrid generating sources it is proposed by researchers to introduce an additional impedance in the system during the fault. Such an introduction is achieved using bridge type fault current limiters. In this paper, authors have compared the performance of series resonance type fault current limiter with capacitive bridge type fault current limiter (CBFCL) and parallel resonance bridge type fault current limiter (PRBFCL). The single-phase representation of the series resonance FCL is shown in Fig. 3.

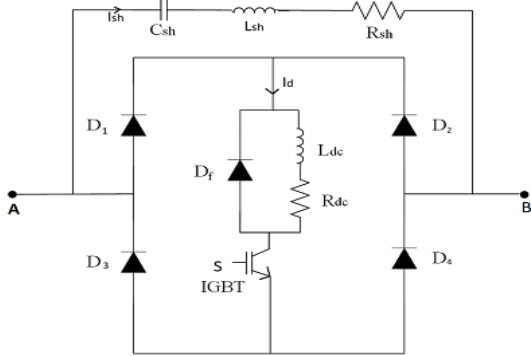


Fig. 3. Single-phase representation of the modified series resonance type FCL

The primitive concept of series resonance-based FCL is found in [19, 20] for stability improvement of synchronous generator based power systems. The authors of [19] have proposed the concept of series resonance type of FCL using a surge arrester, inductor, and capacitor, while in [20] authors have demonstrated the technique of estimating parameters of resonance type FCL for protection and stability analysis of power system having synchronous generators. The authors have modified the topology of [19] by replacing the surge arrester with the resistor for energy dissipation and the rest part of the paper is referred to as the modified series resonance type fault current limiter (MSRFCL). The MSRFCL consists of a bridge section and shunt path. The bridge part comprises diode bridge $D_1 - D_4$, an IGBT switch, a small valued dc reactor L_{dc} with internal resistance R_{dc} , and a parallel free-wheeling diode (D_f). The shunt path comprises a series combination of a resistor R_{sh} , inductor L_{sh} and capacitor C_{sh} as shown in Fig. 3. The resistor R_{sh} is used to limit the current and to dissipate the excess energy from the system during the fault. The inductor L_{sh} limits the rate of rise of line current during the fault and the capacitor C_{sh} helps to improve reactive power support to the system.

In the steady-state condition, the IGBT switch is closed and in positive half cycle of the electrical frequency the line current flows through the path A - D_1 - L_{dc} - R_{dc} - S - D_4 - B while during the negative half cycle the line current flows through A - D_3 - S - R_{dc} - L_{dc} - D_2 - B path. As the current through L_{dc} and R_{dc} flows in the same direction this current is dc. In the steady-state condition, the entire line current will flow from the bridge path of the system as the impedance of the shunt path is very high. The dc reactor is used to limit the rate of rise of

line current at the instance of the fault and saves the IGBT switch from high di/dt.

For designing the controller of the MSRFCL, four parameters are taken into consideration: dc current i_d , permissible reference current (i_T), PCC voltage (V_{pcc}), and the permissible reference voltage (V_T). The controller layout is shown in Fig. 4.

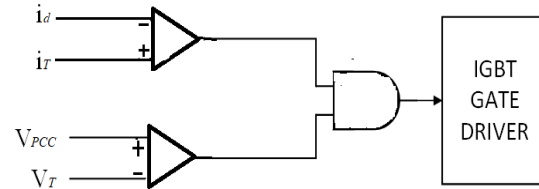


Fig. 4. Control strategy of IGBT switch.

The control circuit comprises two comparators (one each for current and voltage) and an AND gate. The comparator's output is high when i_d is less than or equal to i_T and V_{pcc} is greater than V_T , and during these conditions both the inputs to the AND gate are high and IGBT switch is closed. The value of the permissible reference current i_T is set to nearly 1.3 times the value of dc current. If the i_T is kept more than 1.5 times of i_d the system's response will be delayed and it will allow a large current to flow from the bridge path. On the other side, if the i_T is kept near to 1.15 times of i_d than the system may get false responses because of the transients in the system. The preset reference voltage V_T is set to 0.90 p.u. of the nominal PCC voltage V_{pcc} . At the instance of fault, the dc current i_d rises above the preset permissible reference current i_T , and at the same time the PCC voltage too falls below V_T . The control circuit detects this changed output of AND gate from high to low and opening the IGBT switch. The high fault current of the system gets bypassed through the shunt path, and the fault current is reducing because of the resistor R_{sh} where the energy is dissipated (as C_{sh} and L_{sh} undergo series resonance). The stored energy in inductor L_{dc} is discharged through the free-wheeling diode D_f . Once the protective circuit breaker isolates the faulty part, the system starts recovering and bus voltage at PCC is getting re-instated. On the removal of faults, the circuit breaker re-closes its contacts and the current and voltage comparator checks the respective inputs and the gate signal is provided to re-close the IGBT switch in the bridge part. The system thus returns to the normal operating condition.

In this paper, the authors have considered the capacitive bridge type fault current limiter (CBFCL) [23] and parallel resonance bridge type fault current limiter (PRBFCL) [8] for the comparison of the results. Fig. 5 shows the single-phase representation of CBFCL and Fig. 6 shows the single-phase representation of PRBFCL.

Both CBFCL and PRBFCL consist of the same bridge circuit as discussed in the MSRFCL. The only difference is in the shunt path. As seen in Fig. 5 in the case of CBFCL, the shunt path consists of resistor R_{sh} and capacitor C_{sh} . On the other side, the PRBFCL consists of two shunt paths as seen from Fig. 6. The upper shunt path consists of resistor R_1 and inductor L_{sh} and the lower shunt path consists of resistor R_2 and capacitor C_{sh} . The authors have used the same control strategy for IGBT switch operation for all the FCLs discussed in

this paper. In PRBFCL [8] only PCC voltage is compared with the reference voltage, in this paper current and voltage signals have been used for controlling the operation of IGBT switch. Hence, the PRBFCL is termed as modified PRBFCL (MPRBFCL) in this paper.

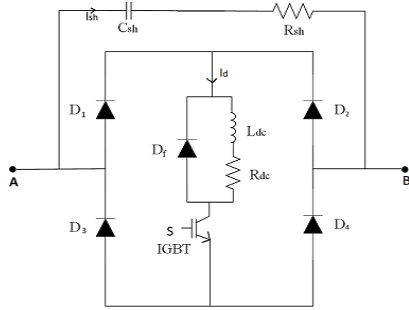


Fig. 5. Single-phase representation of CBFCL.

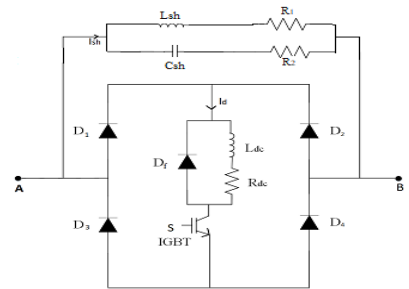


Fig. 6. Single-phase representation of PRBFCL.

IV. MODIFIED WSCC 3 GENERATOR 9 BUS SYSTEM

The behaviour of the power system consisting of different types of generators shall be observed for the system-level fault at one of the load buses. For addressing this issue, in this paper WSCC 3-generator 9-bus system shown in [27] is modified to accommodate the DFIG wind farm and PV solar farm as shown in Fig. 7.

Bus 1 is a swing bus and under the steady-state condition, the power output from all the generators is 72 MW, 163 MW and 85 MW respectively. To consider the large penetration renewable energy-based generation, the synchronous generator at bus 2 is replaced by an equivalent capacity of coherent aggregated DFIG wind farm and the synchronous generator at bus 3 is replaced by the equivalent capacity of aggregated PV solar farm. The proposed FCL is connected between buses 5 and 7. The bus 5 is a weak bus in this system.

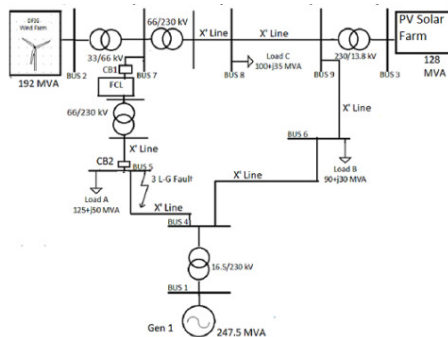


Fig. 7. Modified WSCC 3 generator 9 bus system.

The transient stability performance of the MSRFCL is compared with the CBFCL and MPRBFCL. The modified WSCC system is simulated in the PSCAD / EMTDC software and the system frequency is 60 Hz. For transient stability analysis, wind speed of 11 m/s and solar irradiation of 1000 W/m² is considered and it is assumed to be constant for the fault duration. The fault is simulated at the instant of 10s and fault duration is 150 ms. The relevant circuit breakers CB₁ and CB₂ of the faulty line opens at 10.1s and re-closes successfully after the fault removal at 10.65s.

V. SELECTION OF PARAMETERS FOR FCL

The selection criteria for R_{sh} is considered based on expressions given in [8,23]. P_{sh} is the active power to be dissipated by shunt path at the instant and for the duration of the fault. The series capacitor value (in shunt path of the bridge) is selected so as to suffice the reactive power requirement of system post fault clearance. The power flow in the transmission line connecting bus 7 and bus 5 is 84 MW under steady-state condition.

The current from shunt path I_{sh} is given by

$$I_{sh} = [84 \text{ MW} / (66 \text{ kV} \cdot \sqrt{3})] = 735 \text{ A}$$

Based on the value of I_{sh}, the resistance of shunt path R_{sh} is calculated as:

$$R_{sh} = [84 \text{ MW} / (735 \cdot 735)] = 155 \Omega$$

Hence, per phase value of R_{sh} turns out to be 51.83 Ω and it is selected as 52 Ω. As the system consists of the wind farm and PV solar farm, the capacitance of the shunt path C_{sh} is selected as 100 μF per phase and based on the concept of resonance L_{sh} is derived as 70 mH. The ratio of L_{dc} / R_{dc} is considered as 10 for all the types of FCLs. To compare the results of CBFCL and MPRBFCL with the MSRFCL, R_{sh} is selected as 52 Ω and C_{sh} is selected as 100 μF per phase in the case of CBFCL. In the case of PRBFCL R₁ and R₂ are selected as 165 Ω and 69.69 Ω respectively based on the calculation given [8] while the capacitor value and inductor value are selected as 100 μF and 70 mH respectively.

VI. SIMULATION RESULTS AND COMPARISON OF VARIOUS FCLs

The following cases are considered for the transient stability analysis of the modified multi-machine power system.

- (1) Transient stability analysis without any controller.
- (2) Transient stability analysis with CBFCL.
- (3) Transient stability analysis with MPRBFCL.
- (4) Transient stability analysis with MSRFCL.

To show the performance comparison of the FCLs for system-level fault, the three-line-to-ground (3LG) fault is simulated at weak bus 5 of the system. The response of RMS line voltage, active power, reactive power and RMS current of all the three generators at bus 1, 2 and 3 are presented and analyzed.

Fig. 8 shows the RMS line voltages of all generators at bus 1, 2 and 3 during pre-fault, fault and post fault condition.

The RMS line voltage in steady-state condition is 1 pu. In the event of symmetrical fault at bus 5, the voltage at Bus 2 falls to 0.34 pu when no FCL is connected in the system. With the FCL installed in the system, the voltage profile at all the generator buses is improved significantly. At bus 2, with the MSRFCL, the voltage

improves to 0.85 pu as compared to 0.81 pu in the case with CBFCL. In the case of MPRBFCL, the voltage improves to 0.88 pu and the voltage variation range is same to series resonance FCL. In the case of MSRFCL, the RMS voltage varies in the band between 0.85 pu to 1.09 pu while in MPRBFCL it varies in the band of 0.88 pu to 1.12 pu.

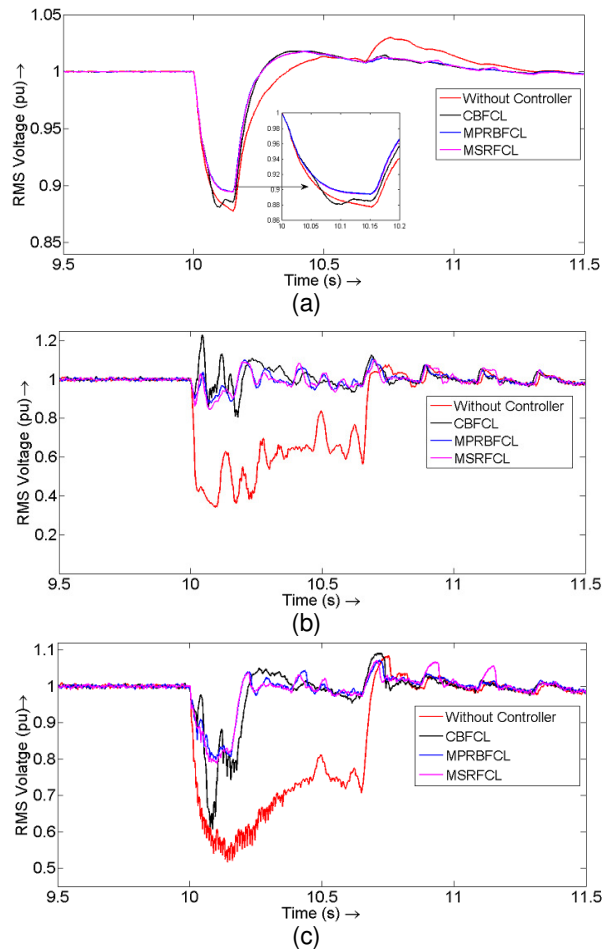


Fig. 8. RMS line voltages at generator buses for 3 L-G fault (a) bus1 (b) bus2 (c) bus 3.

It is evident from Fig. 8 (b) that the insertion of the inductor with the capacitor leads to reduced voltage swing on all the generator buses. The effect on generator 1 is insignificant as it is a swing generator with a very large capacity (Fig. 8 (a)). The RMS voltage at generator 3 is improved from 0.52 pu for the case of no FCL to 0.79 pu with MSRFCL and MPRBFCL as seen from Fig. 8(c) which is better than CBFCL.

Fig. 9 shows the active power output at generator buses 1, 2 and 3 in pre-fault, fault and post fault condition.

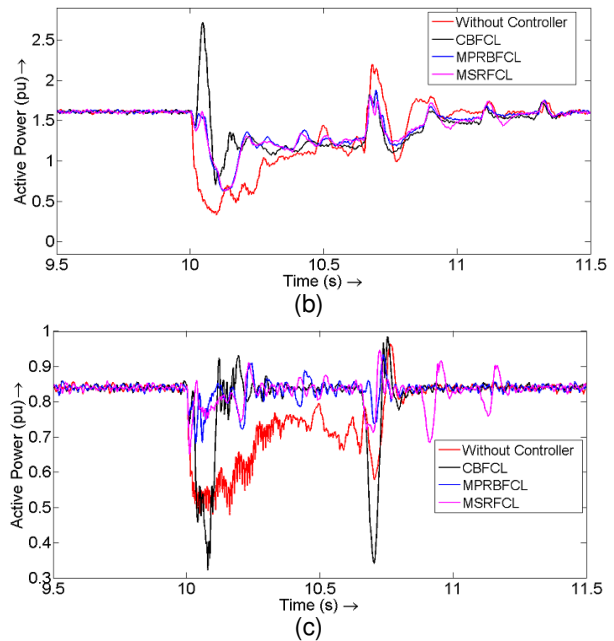
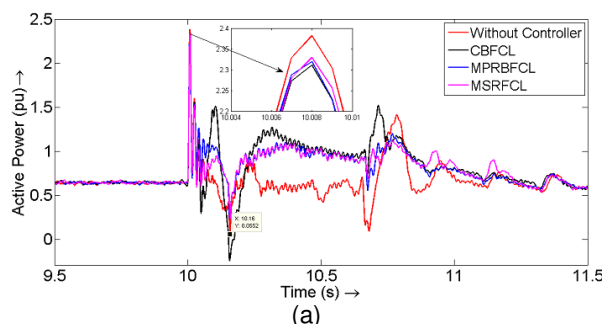
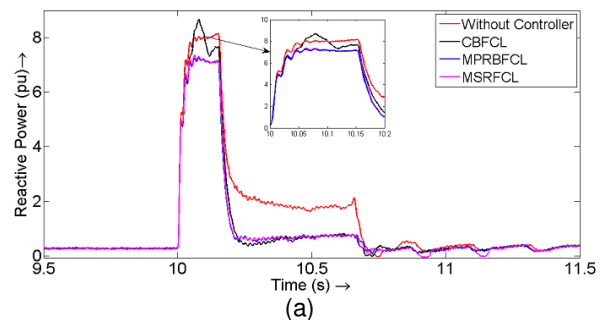


Fig. 9. Active power output at generator buses for 3 L-G fault (a) bus1 (b) bus2 (c) bus 3.

The active power output from generator 2 in its steady-state condition is 1.63 pu at bus-2. As seen from Fig. 9 (b), the active power output during fault at bus 2 dips to 0.34 pu in case where no FCL is installed in the system. With the FCL connected in the system, the active power output of generators improves significantly during the fault. Apparent from the graphs of Fig. 9 (b), MSRFCL gives less power swing as compared to all other FCLs. As seen in Fig. 9 (a), generator 1 supplies active power even during the fault interval with the MSRFCL and the power swing is also less as compared to all other FCLs. A careful investigation shows that with the MSRFCL the variation in active power output of generator 3 is also reduced as compared to the case of CBFCL Fig. 9 (c). Fig. 10 represents the reactive power at generator buses. The variation in reactive power is also reduced at all the buses with FCLs. It is noted that being R-C network the CBFCL contributes more reactive power at bus 2 as seen from Fig. 10 (b), bringing greater swing in RMS voltages at bus 2 in case of the case of CBFCL which is evident from Fig. 8 (b). Fig. 10 (a) and Fig. 10 (c) shows the reactive power at bus 1 and bus 3 respectively. In this case also, CBFCL supplies more reactive power as compared the MSRFCL and MPRBFCL during the fault condition.



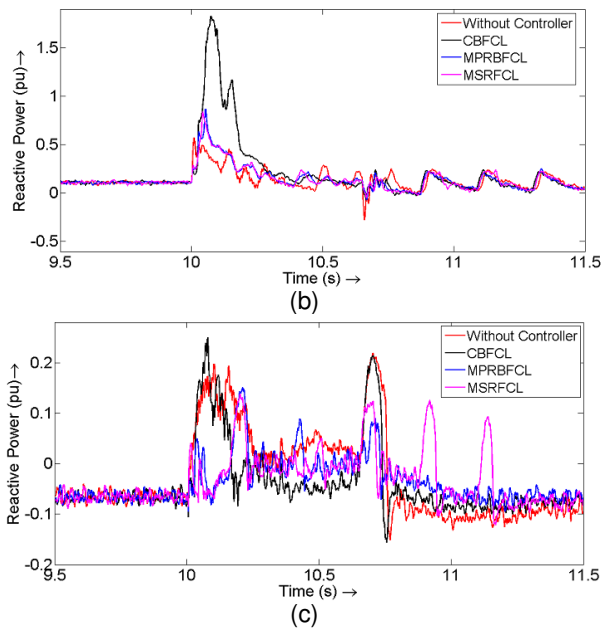


Fig. 10. Reactive power output at generator buses for 3 L-G fault (a) bus1 (b) bus2 (c) bus 3.

Fig. 11 shows a comparison of RMS currents at the generator buses. In the fault condition, the peak value of the RMS current shoots to 2.56 pu from its base value of 1.63 pu in the absence of a series device at bus 2, which is limited 2.21 pu with the MSRFCL, better as compared to CBFCL and MPRBFCL.

The results of bus 1 is almost similar for all the cases of FCLs. In the case of bus 1 the peak value current in the case of CBFCL is slightly lower than MSRFCL, but the oscillations are very high than the MSRFCL. At bus 3 where the base current is 0.85 pu, during the fault the peak value of current touches 1.10 pu for the case of no FCL and improves to 1 pu in MSRFCL which is better than CBFCL and MPRBFCL as seen in Fig. 11. (c).

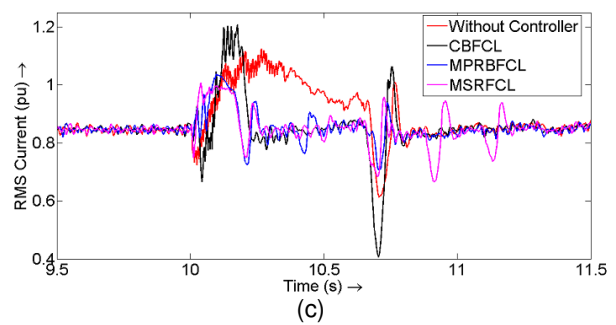
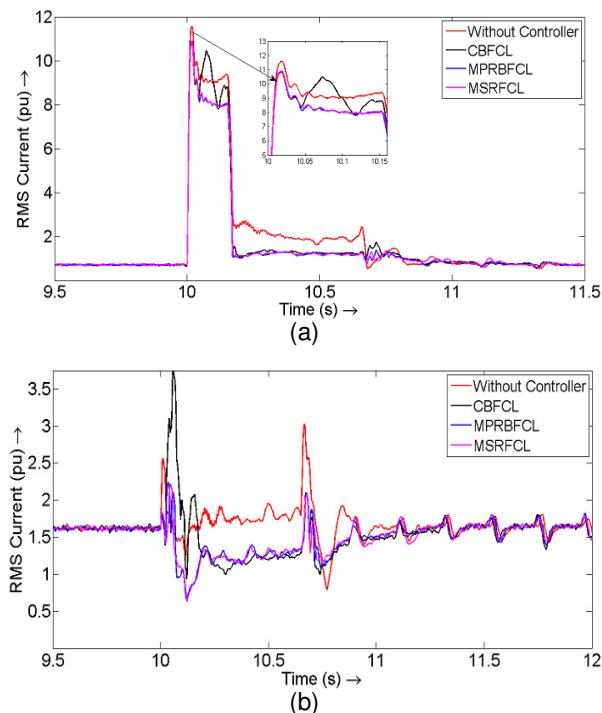


Fig. 11. RMS line current at generator buses for 3 L-G fault (a) bus1 (b) bus2 (c) bus 3

Result comparison: The following tables show the comparison of all the performance indicators of various FCLs used in this paper.

Table 1: Comparison of performance parameters at Bus 1.

Quantity FCL	V_1 (rms) (Voltage dip) pu	P_1 range Pu	Q_1 (peak) pu	I_1 (rms) (peak) pu
No controller	0.87	0.05 to 2.38	8.16	11.58
CBFCL	0.88	-0.23 to 2.31	8.67	10.83
MPRBFCL	0.89	0.23 to 2.32	7.28	10.89
MSRFCL	0.89	0.23 to 2.33	7.36	10.87

Table 2: Comparison of performance parameters at Bus 2.

Quantity FCL	V_2 (rms) (voltage dip) pu	P_2 Range pu	Q_2 (peak) pu	I_2 (rms) (peak) pu
No controller	0.34	0.34 to 2.20	0.57	2.56
CBFCL	0.81	0.70 to 2.71	1.83	3.73
MPRBFCL	0.88	0.63 to 1.88	0.86	2.23
MSRFCL	0.85	0.63 to 1.81	0.85	2.21

Table 3: Comparison of performance parameters at Bus 3.

Quantity FCL	V_3 (rms) (Voltage dip) pu	P_3 Range pu	Q_3 (peak) pu	I_3 (rms) (peak) pu
No controller	0.52	0.48 to 0.96	0.21	1.10
CBFCL	0.61	0.32 to 0.99	0.25	1.20
MPRBFCL	0.79	0.68 to 0.94	0.15	1.03
MSRFCL	0.79	0.66 to 0.94	0.14	1.00

VII. CONCLUSION

The paper focuses on the transient stability analysis of a multi-machine power system with high penetration of renewable energy sources. The equal capacity of aggregated DFIG based wind farm and PV solar farm are chosen to replace synchronous machines in a standard WSCC test system. Deviating from the usual SMIB performance alone, the authors have discussed the effect of system-level fault at the weak bus in a multi-machine system to validate and compare the results of MSRFCL with CBFCL, MPRBFCL and the case where no FCLs are connected in the system. From the simulation results, the following are noteworthy points.

1. The insertion of FCLs in the multi-machine system improves the voltage profile of the system and also reduces the peak value of fault current of the system as compared with the case where no FCLs are connected in the system.

2. The results of the MSRFCL and MPRBFCL are similar for the majority of cases, the construction of MPRBFCL requires 2 shunt paths and 2 different values of resistors whereas the MSRFCL requires only 1 shunt path. The construction of MSRFCL is simple as compared to MPRBFCL.

3. The authors have shown the effect on the other synchronous generator connected at bus 1 and solar farm connected at bus 3. From the presented results, it is observed that the performance of solar farm at bus 3 is improved with the MSRFCL as compared to CBFCL and the results are similar in the case of MPRBFCL. Based on the above points it can be concluded that proposed MSRFCL not only enhances transient stability of the multi-machine hybrid power system but also improves the low voltage ride through the performance of the power system with hybrid generating sources.

VIII. FUTURE SCOPE

The authors have compared various types of fault current limiters for 3L-G fault at the weak bus in a multi-machine system. The observations for asymmetrical fault (L-G, L-L and L-L-G) conditions may offer a good insight in the performance analysis of FCLs.

ACKNOWLEDGEMENTS

Both authors have contributed equally on this manuscript together and both authors have read and approved the final manuscript.

Funding: This research received no external funding.

Conflict of Interest. The authors declare no conflict of interest.

REFERENCES

- [1]. Hammons, T.J. (2008). Integrating renewable energy sources into European grids. *International Journal of Electrical Power Energy Systems*, 30, 462-475.
- [2]. Ngamroo, I. (2017). Review of DFIG wind turbine impact on power system dynamic performances. *IEEE Transactions on Electrical and Electronic Engineering*, 12(3), 301-311.
- [3]. Brahmendra Kumar, G. V., Sarojini, R. K., Palanisamy, K., Padmanaban, S., & Holm-Nielsen, J. B. (2019). Large scale renewable energy integration: Issues and solutions. *Energies*, 12(10).
- [4]. Rakhshani, E., Rouzbehi, K., Adolfo, J. S., & Tobar, A. C. (2019). Integration of Large Scale PV-Based Generation into power systems: A survey. *Energies*, 12(1425).
- [5]. Pena, R., Cardenas, R., & Asher, G. (2013). Overview of control systems for the operation of DFIGs in wind energy applications. *IEEE Transactions on Industrial Electronics*, 60(7), 2776-2798.
- [6]. Ezzat, M., Benbouzid, M., Muyeen, S. M., & Harnefors, L. (2013). Low-voltage ride-through techniques for DFIG-based wind turbines: State-of-the-art review and future trends. *IECON Proceedings (Industrial Electronics Conference)*, 7681-7686.
- [7]. Liserre, M., Cárdenas, R., Molinas, M., & Rodríguez, J. (2011). Overview of multi-MW wind turbines and wind

parks. *IEEE Transactions on Industrial Electronics*, 58(4), 1081-1095.

- [8]. Hossain, M. K., & Ali, M. H. (2016). Transient stability augmentation of PV/DFIG/SG-based hybrid power system by parallel-resonance bridge fault current limiter. *Electric Power Systems Research*, 130, 89-102.
- [9]. Bak, Y., Lee, J. S., & Lee, K. B. (2018). Low-voltage ride-through control strategy for a grid-connected energy storage system. *Applied Sciences (Switzerland)*, 8(1)
- [10]. Patel, S. H., Yadav, R. K. and Joshi, D. Y. (2020). Impacts of FACTs on Distributed Generation System. *International Journal on Emerging Technologies*, 11(2): 633-636.
- [11]. Sengupta, S., Kumar, A., & Tiwari, S. (2018). Transient stability enhancement of a hybrid Wind-PV farm incorporating a STATCOM. *2018 3rd IEEE International Conference on Recent Trends in Electronics, Information and Communication Technology, RTEICT 2018 - Proceedings*, 1574-1580.
- [12]. Mohanty, A., Viswavandya, M., Ray, P. K., & Mohanty, S. (2018). Back stepping sliding mode control for transient voltage stability in standalone hybrid power system: An experimental analysis. *Proceedings of 2018 IEEE International Conference on Power Electronics, Drives and Energy Systems, PEDES 2018*, 1-6.
- [13]. Mathew, L., & Chatterji, S. (2016). Modeling and simulation of hybrid power flow controller implemented on Multi-Machine system. *2015 2nd International Conference on Recent Advances in Engineering and Computational Sciences, 2015*, 1-6.
- [14]. Shah, P., & Singh, B. (2019). LVRT capabilities of solar energy conversion system enabling power quality improvement. *2019 IEEE International Electric Machines and Drives Conference, IEMDC 2019, 110016*, 2083-2088.
- [15]. Islam, G. M. S., & Al Durra, A. (2015). LVRT capability improvement of a grid-connected PV park by robust sliding mode control. *Proceedings of the American Control Conference, 2015-July*, 1002-1009.
- [16]. Movahedi, A., Niasar, A. H., & Gharehpetian, G. B. (2019). LVRT improvement and transient stability enhancement of power systems based on renewable energy resources using the coordination of SSSC and PSSs controllers. *IET Renewable Power Generation*, 13(11), 1849-1861.
- [17]. Li, Z. E., Tiong, T. C., & Wong, K. I. (2019). Improving Transient Stability of Diesel-Wind-Solar Hybrid Power System by using PSS. *2019 IEEE International Conference on Electrical, Control and Instrumentation Engineering, ICECIE 2019 - Proceedings*, (2), 2-7.
- [18]. Ghanasyam, P., Verma, A., & Mitra, A. (2018). Impact of Hybrid Renewable Sources on the Transient Stability of Multi-machine Power System. *Proceedings of 2018 IEEE International Conference on Power Electronics, Drives and Energy Systems, PEDES 2018*, 1-5.
- [19]. Hagh, M. T., Naderi, S. B., & Jafari, M. (2010). New resonance type fault current limiter. *PECon2010 - 2010 IEEE International Conference on Power and Energy*, 507-511.
- [20]. Sirisha, A. N. R. L., & Pradhan, A. K. (2017). Parameter Estimation of Resonant Fault Current Limiter for Protection and Stability Analysis. *IEEE Transactions on Power Systems*, 32(3), 2288-2295.

- [21]. Hossain, M. E. (2017). A non-linear controller based new bridge type fault current limiter for transient stability enhancement of DFIG based Wind Farm. *Electric Power Systems Research*, 152, 466–484.
- [22]. Rashid, G., & Ali, M. H. (2015). Transient Stability Enhancement of Doubly Fed Induction Machine-Based Wind Generator by Bridge-Type Fault Current Limiter. *IEEE Transactions on Energy Conversion*, 30(3), 939–947.
- [23]. Firouzi, M., & Gharehpetian, G. B. (2018). LVRT Performance Enhancement of DFIG-Based Wind Farms by Capacitive Bridge-Type Fault Current Limiter. *IEEE Transactions on Sustainable Energy*, 9(3), 1118–1125.
- [24]. Abdel-Baqi, O., & Nasiri, A. (2011). Series voltage compensation for DFIG wind turbine low-voltage ride-through solution. *IEEE Transactions on Energy Conversion*, 26(1), 272–280.
- [25]. Kundur, P. (2006). Power System Stability and Control, *McGraw-Hill*.
- [26]. Sauer, P.W., & Pai, M.A. (2007). Power System Dynamics and Stability, *Prentice Hall*.
- [27]. Anderson, P.M., Fouad, A.A. (2008). Power System Control and Stability, *Iowa State University Press*.

How to cite this article Mehta, C. R. and Vora, S. C. (2020). Transient Stability Enhancement of Multi-Machine Hybrid Power System Employing Modified Series Resonance type Fault Current Limiter. *International Journal on Emerging Technologies*, 11(3): 858–866.